The FLOWLENS: A Focus-and-Context Visualization Approach for Exploration of Blood Flow in Cerebral Aneurysms

Rocco Gasteiger, Mathias Neugebauer, Oliver Beuing, and Bernhard Preim
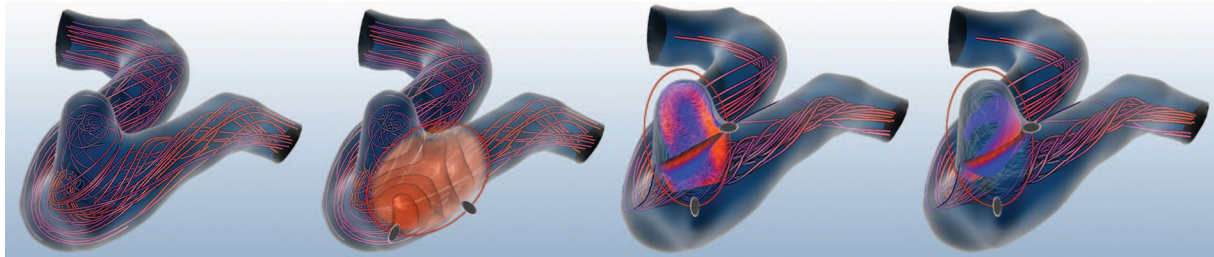

Fig. 1. Various applications of the FLOWLENS (red ellipse) for the exploration of blood flow in cerebral aneurysms.

Abstract—Blood flow and derived data are essential to investigate the initiation and progression of cerebral aneurysms as well as their risk of rupture. An effective visual exploration of several hemodynamic attributes like the wall shear stress (WSS) and the inflow jet is necessary to understand the hemodynamics. Moreover, the correlation between focus-and-context attributes is of particular interest. An expressive visualization of these attributes and anatomic information requires appropriate visualization techniques to minimize visual clutter and occlusions. We present the FLOWLENS as a focus-and-context approach that addresses these requirements. We group relevant hemodynamic attributes to pairs of focus-and-context attributes and assign them to different anatomic scopes. For each scope, we propose several FLOWLENS visualization templates to provide a flexible visual filtering of the involved hemodynamic pairs. A template consists of the visualization of the focus attribute and the additional depiction of the context attribute inside the lens. Furthermore, the FLOWLENS supports local probing and the exploration of attribute changes over time. The FLOWLENS minimizes visual cluttering, occlusions, and provides a flexible exploration of a region of interest. We have applied our approach to seven representative datasets, including steady and unsteady flow data from CFD simulations and 4D PC-MRI measurements. Informal user interviews with three domain experts confirm the usefulness of our approach.

Index Terms—Flow Visualization, Focus-and-Context, Illustrative Rendering, Aneurysm.

---

1 INTRODUCTION

Cerebral aneurysms result from a congenital or evolved weakness of stabilizing parts of the vessel wall and leads to a local dilatation with a saccular or fusiform shape. They have a prevalence of about 2% [7] in Western Europe and bear a high risk of rupture with often fatal consequences for the patient. A rupture results in a subarachnoid hemorrhage which has a fatality rate of up to 52% [18]. The treatment of cerebral aneurysms aims to induce thrombus formation based on an endovascular procedure to seal them [1]. Aneurysm formation, evolution and risk of rupture involve hemodynamics, wall biomechanics [30, 34], extravascular environment, aneurysm morphology, genetics and other clinical and epidemiological factors. Hemodynamic attributes like WSS, vorticity, and jetting play an important role in the inception and later development of aneurysms [2, 35].

Based on the patient-specific aneurysm anatomy, biomedical researchers employ computational fluid dynamic (CFD) simulations and acquire 4D phase-contrast MRI (4D PC-MRI) data to investigate the aneurysm initiation, progression and assessment of the risk of rupture [3, 10, 23]. Because of the increased computational power,

the availability of advanced simulation models and image acquisition modalities, medical researchers are capable of studying the 3D hemodynamic within the aneurysm [2, 6, 10, 11, 23].

The obtained flow data consists of several relevant hemodynamic attributes like flow velocity, WSS and flow pattern. These data are very complex and domain experts (biomedical researchers and clinicians) need support to explore such data. In addition to a quantitative analysis, such as measurements of the geometry and hemodynamic attributes, an effective visual exploration of these attributes is important to obtain insights of the hemodynamic characteristics. Existing approaches present these data either in a multiparameter visualization or in a side-by-side view of the individual attributes. The advantage of a multiparameter visualization consists of the direct spatial correlation between several attributes but leads to visual cluttering and occlusions. In a side-by-side view, these two problems are resolved but a high mental effort in terms of the spatial correlation between the attributes is necessary. We present a *picture-in-picture* concept which combines advantages of both approaches. Depending on a specific hemodynamic focus attribute additional information of relevant context attributes are embedded over the same spatial region. Our concept enables a flexible definition of this focus-and-context region and reduces visual cluttering. Since domain experts are not familiar with complex flow visualizations, we incorporate expressive visualization templates of the hemodynamic attributes to reflect the domain experts' needs and habits.

Summarizing, the main contributions of this paper are:

- We give an overview about relevant hemodynamic attributes for the assessment of cerebral aneurysms. These attributes are assigned to three anatomic scopes. In each scope, we group attributes to pairs of focus-and-context attributes relevant for the

- *Rocco Gasteiger, Mathias Neugebauer and Bernhard Preim are with the department of Simulation and Graphics, within the group Visualization at the University of Magdeburg, Germany,*
  Email: {rocco.gasteiger, mathias.neugebauer, bernhard.preim} @ovgu.de.
- *Oliver Beuing is with the department of Neuroradiology at the University Hospital Magdeburg, Germany, E-mail: oliver.beuing@med.ovgu.de.*

visual exploration.

- We introduce the FLOWLENS as an interactive 2D widget to provide a flexible visual filtering for the visualization of the focus-and-context pairs. The lens supports local probing and conveys changes over time for the lens region.

- For each focus-and-context pair, we propose different FLOWLENS visualization templates by employing existent flow and multiparameter visualization techniques. A template consists of the visualization of the focus attribute and the additional depiction of the context attribute inside the lens. Thereby, we consider a minimum of adjustable parameters and visual complexity as well as an enhancement of spatial perception.

- Informal user interviews with three domain experts are conducted to assess the FLOWLENS visualization concept in terms of the visual exploration.

2 RELATED WORK

The visual exploration of blood flow data gains importance due to the increased availability of measured and simulated blood flow data. Major application areas are investigations of cardiovascular and cerebral systems. Biomedical researchers employ established flow visualization techniques, like color-coded streamlines, pathlines, stream surfaces and glyphs [2, 6, 23]. For a detailed view on the flow data, e.g., the investigations of the inflow jet into an aneurysm, probe planes are used with a dense or texture-based flow visualization like color coding of several flow scalars or a LIC of the probed flow field [10]. Surface flow data like WSS are depicted by color-coded surface renderings [10]. Interaction and mental effort is necessary to gain an overview about the distribution of the surface data. Neugebauer et al. [27] presented a map display for an intuitive and interactive overview visualization of surface data. They employ a 2D projection of the surface data along with the 3D aneurysm model which increases the ease of use and minimizes mental effort.

Established flow visualization techniques (see Laramee et al. [21] and Salzbrunn et al. [31] for a survey) tend to be visually complex. Hence, there is an increased interest in a simplified representation of the flow data by incorporating illustrative rendering techniques. Mattausch et al. [24] extended illuminated streamlines with halos to improve spatial perception. Depth-dependent halos were introduced by Everts et al. [14] to improve the spatial perception of densely seeded streamlines, generated from DTI fiber tracking. Born et al. [5] employed contour lines, halftoning and illustrative surface streamlines for an expressive visualization of complex stream surfaces. Illustrative flow-rate arrows were used by van Pelt et al. [37] to depict time-dependent blood flow in cardiovascular systems. They employed silhouette rendering and toon shading to convey the anatomical context. Our approach is also inspired by illustrative rendering techniques due to its potential of a simple depiction and focusing on relevant information.

The blood flow hemodynamics depends strongly on the enclosing vessel anatomy and consists of multi-variate data. In general, the amount of relevant information is often relatively small compared to the overall amount of acquired data. Hence, the focus-and-context strategy is frequently used to visually differentiate focus information from the spatial context. It aims for a minimization of occlusions and visual cluttering as well as for a flexible visual filtering of the multi-variate data [8, 13, 40]. Focus information are classified (e.g., by importance values) and are enhanced by visual attributes (e.g., color) or by geometrical deformations. Context information are represented attenuated (e.g., by transparency or by illustrative visualization techniques) or are omitted if they occlude focus information. Gasteiger et al. [15] presented a visualization of the enclosing aneurysm surface that depicts important anatomical surface features, whilst simultaneously gaining maximal visibility of the embedded flow visualization. They employ a ghosted view of the vessel surface which modulates the transparency according to the orientation of the

surface normal to the viewer. Ghosted views belong to smart visibility techniques (see Viola et al. [39] for an overview).

In terms of a flexible data filtering we are inspired by the *magic lenses* approach, introduced by Bier et al. [4]. A lens consists of a 2D widget with arbitrary shape rendered over the scene. The shape inside defines the focus region and the shape outside represents the context region. Within the focus region, visual filters may be incorporated to reveal hidden information, to enhance data of interest, or to suppress distracting information of a 2D or 3D scene. Applications can be found, for example, in interactive NPR line drawings [29] and context preserving volume renderings [19, 41]. Viega et al. [38] introduced volumetric lenses (3D magic lenses) and Mattausch et al. [24] employed these lenses to draw regions of 3D flow in greater detail. The aforementioned probe planes are a direct application of the volumetric lens concept. They are used as a common exploration tool to probe the blood flow interactively at specific vessel or aneurysm sections to get a detailed view on the underlying flow behavior [10, 12]. However, an increased interaction effort is necessary to place such probe planes. Van Pelt et al. [37] introduced view-aligned planar reformats of vessel cross-sections to ease probe plane placement. Based on a one-click strategy they compute a local multi-planar reformat and place the cross-section view aligned next to the probed vessel section. Neugebauer et al. [28] presented an anatomy-guided exploration of blood flow in cerebral aneurysms. They used the vessel centerline and derived anatomic landmarks to ease the probe or seed plane placement. They incorporated these landmarks into a multi-scope approach that supports the visual exploration of the flow at different anatomic scopes: a global overview of flow in the aneurysm, the ostium flow profile and the local probing with special widgets for the aneurysm and the parent vessel. However, they do not provide an exploration of near-wall information.

3 ANALYSIS OF HEMODYNAMIC DATA

In the field of medical research, several computational tools are being developed to help biomedical researchers and clinicians in the investigation of aneurysm initiation, growing, and risk of rupture based on hemodynamic data. Without a visualization of these complex data it is not conceivable to understand the correlations between specific hemodynamic characteristics and their influence on the development of the aneurysm. Our approach aims for a support of the visual exploration of aneurysm hemodynamics during that investigation. Thereby, domain experts are interested in a high-level exploration of the data rather than in a detailed and flexible view on the visual representation of that data. Their tasks involve getting an overview of the hemodynamic characteristics as well as findings of correlations, e.g., regions of specific near-wall information and the region of a further aneurysm growing. Hence, the goal of our approach is to provide a high level of usability, automation, and expressive visualization of hemodynamic data. Based on the medical research domain the design of such a visualization system involves several requirement considerations. Before we go into details, we shortly present the medical research pipeline of analyzing hemodynamic data in which our approach is embedded. This pipeline consists of data acquisition, data preprocessing and analysis, illustrated in Fig. 2.

3.1 Data Acquisition

In the first step, clinical image data (CTA, MRA, or 3D rotational angiography) of the aneurysm morphology are acquired. Common clinical resolutions are up to $512 \times 512 \times 140$ with a voxel size of $0.35 \times 0.35 \times 0.9$mm. If 4D PC-MRI (Phase-Contrast-MRI) is available, a full 3D flow measuring over time can be performed, which encodes the flow direction and magnitude at each voxel [23]. Common resolutions for medical research are up to $144 \times 256 \times 128$ with a voxel size of $1 \times 1 \times 1$mm as well as 10 to 20 time points evenly spaced over the cardiac cycle with a temporal resolution of about 90ms.
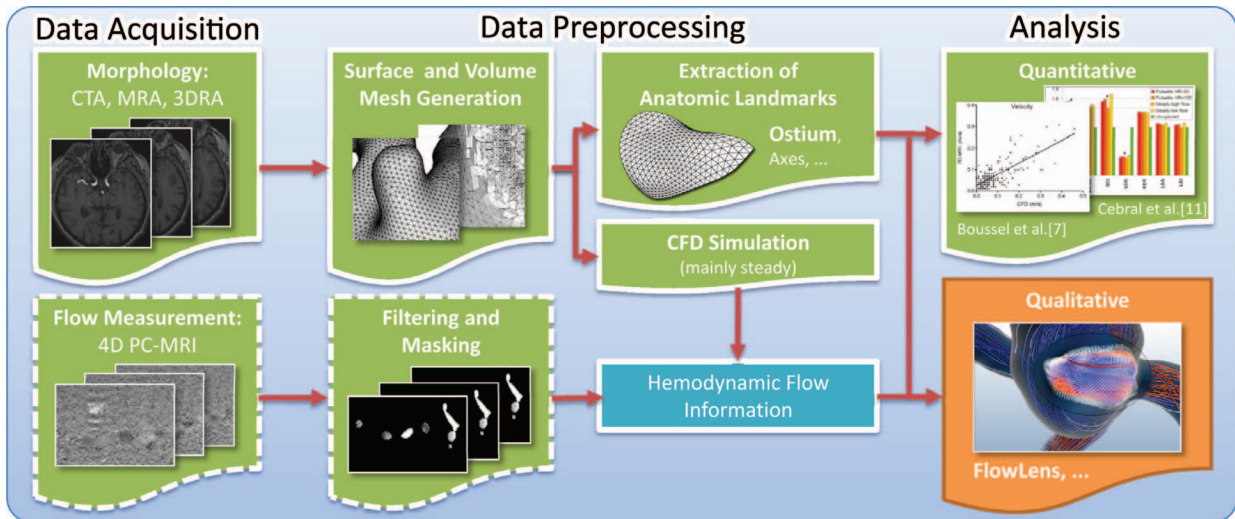
Fig. 2. Overview about the pipeline for analyzing hemodynamic information. The pipeline consists of three steps: in the data acquisition step, clinical image data of the aneurysm are acquired. If 4D PC-MRI is available, a full 3D flow measuring over time can be performed. The obtained data have to be preprocessed in terms of the CFD simulation and error filtering of the measured flow data. The resulting hemodynamic information are then focus of a quantitative and qualitative analysis. The step our approach belongs to is highlighted in orange.

3.2 Data Preprocessing

The preprocessing includes the reconstruction of the vessel surface, the extraction of anatomic landmarks, the generation of simulated flow data as well as filtering of the measured flow data.

Surface Reconstruction: For the reconstruction of the vessel surface, a segmentation of the aneurysm and its parent vessel is necessary. Because of the high vessel-to-tissue contrast in the image data often a simple thresholding segmentation followed by a connected component analysis is sufficient to separate the aneurysm and its parent vessel from the surrounding tissue. More advanced techniques like active shape models and deformable models can be employed to minimize manual effort in cases of low intensity distribution [22]. Based on the segmented mask, the surface mesh of the aneurysm is reconstructed with Marching Cubes and optimized with respect to mesh quality by a combination of metric and topological changes like edge collapses and edge flips (for details see [33]).

Extraction of Anatomic Landmarks: In addition to the vessel surface anatomic landmarks are extracted like the ostium (surface area which separates the aneurysm from the parent vessel) or the central aneurysm axis (CAS) [26]. Domain experts utilize these landmarks to explore local flow changes.

Generating Simulated Flow Data: The optimized surface mesh is used for generating a volume mesh which is the input for the subsequent CFD simulation. In most cases, the blood is modeled as Newtonian fluid with steady or unsteady flow and rigid walls. Cebral et al. have shown that with these assumptions a qualitative flow characterization is still possible [9].

Filtering and Masking Measured Flow Data: If 4D PC-MRI flow data was acquired, measuring errors introduced by eddy currents, noise and velocity phase wraps are reduced according to several filter methods described in Hennemuth et al. [16]. Subsequently, several hemodynamic attributes like WSS and flow pressure are derived from the flow field [11].

3.3 Analysis

The preprocessing of the data enables the quantitative and qualitative analysis of relevant hemodynamic information as well as the anatomy. The quantitative analysis focuses on statistical evaluations of hemodynamic and geometric information (e.g., ratio of mean hemodynamic attributes) in terms of aneurysm evolution and rupture [11, 17, 35]. Our approach belongs to the qualitative analysis, which involves the visual exploration of hemodynamic and geometric information (highlighted

box in Fig. 2). The qualitative analysis involves the exploration of the surface, near-wall information, surface and flow, anatomy-guided flow (e.g., at the ostium), and flow topology. Our approach supports the exploration of near-wall information, embedded flow and anatomy-guided flow.

4 REQUIREMENT ANALYSIS

We intend to provide an effective visual exploration of the blood flow hemodynamics in cerebral aneurysms. This goal is ambitious due to the complex nature of the data and the fact that the target user group cannot be assumed to be familiar with advanced flow visualization techniques. Hence, we derived the following requirements regarding the habits and needs of domain experts with a series of interviews, observations and scenario discussions. The requirements have been verified by analyzing medical publications such as [10, 34].

4.1 Hemodynamic Information and Spatial Scopes

To support domain experts in their visual exploration of the hemodynamics, we first have to identify relevant hemodynamic attributes. These attributes refer to different spatial scopes of the aneurysm. Furthermore, domain experts investigate correlations between a focus attribute and a context attribute at a specific spatial scope of the aneurysm. For instance, they compare the flow with the WSS distribution on the surface to investiage the influence of the flow behavior to the WSS magnitude. Hence, the definition of spatial scopes and the assignment of corresponding focus-and-context pairs to these scopes are important to steer the exploration process.

4.2 Ease of Use

Based on the spatial scopes together with their pairs of hemodynamic attributes, we aim at a comfortable visual exploration of these information. This includes the following aspects:

Simplicity: The visualization must be as simple as possible to minimize visual cluttering and occlusions. For each spatial scope, we shall represent the relevant hemodynamic attributes with established visualization techniques. This involves visualization templates with default parameter settings, a wide-spread concept. In terms of color mapping, we consider domain-specific habits, e.g., warm colors for high values and blue colors for low values.

Focus-and-Context: The visual representation of hemodynamic attributes for a given spatial scope corresponds to a multiparameter visualization. The simultaneous visualization of *all* attributes is not desired by the domain experts. Based on a given focus attribute they want

to investigate correlations to other attributes as context, especially at spatial locations of the aneurysm where the focus attribute has some specific characteristics. As an example, they want to investigate the flow at vessel regions where high WSS occurs. For such a visual filtering on demand, a flexible focus-and-context approach with a simple interaction scheme is necessary. Thereby, we do not consider multiview approaches which consist of several side-by-side views each with a single visualization of a specific attribute. Although a minimum of visual clutter is given, these approaches exhibit an increased mental effort in terms of spatial correlations for the viewer.

Probing: Domain experts are also interested in drawing hemodynamic attributes in detail at particular locations of the aneurysm, e.g., the velocity at a vessel cross-section. Probing relates to this requirement by resampling the flow dataset with a probe dataset (e.g., a plane or a volume). It can be used to reduce data or to view data in a particular fashion. Care must be taken with respect to the sampling resolution to avoid missing important high-frequency information or false confidence. Furthermore, a user-friendly placement must be provided to minimize interaction effort.

5 FLOWLENS CONCEPT

In the following, we present our general concepts to achieve the requirements described in Sec. 4. We first indentify relevant hemodynamic attributes, based on a review of current medical research. Based on the five exploration steps of the qualitative analysis (recall Sec. 3.3), we assign the identified hemodynamic attributes to spatial scopes and compose each attribute to pairs of focus-and-context attributes. For each scope, we propose templates of focus-and-context visualizations to represent the involved pairs of hemodynamic attributes. Note that we do not focus on developing new flow visualization techniques but on representing each pair in an optimal way based on existing techniques. To avoid visual clutter and occlusions, we introduce the FLOWLENS as a flexible visual filtering approach. During the visual exploration of a focus attribute, the FLOWLENS can be placed over a spatial region where the correlation to its context attribute is of interest. Within the lens, the visualization of the focus attribute is then attenuated and the visualization of the context attribute is shown.

5.1 Identification of Hemodynamic Attributes

We have identified six attributes that medical researchers have recently used to investigate the correlation between hemodynamic attributes and aneurysm initiation, progression and rupture [2, 3, 10, 30, 34]. We explain them briefly and assign them later to spatial scopes. Within each scope the attributes are combined to pairs of focus-and-context attributes. These pairs represent the content displayed in the FLOWLENS.

The embedded *flow* is used to gain a first impression of the qualitative flow behavior, e.g., amount of aneurysm inflow and flow complexity. It is characterized by flow direction and velocity. Flow with low velocity within the aneurysm also indicates a thrombus formation. A more detailed view on the flow pattern is described by the *grade of vorticity*. Studies have shown that aneurysms with complex and unstable flow patterns bear an increased risk of rupture [2, 10]. Furthermore, it is known that *WSS* has an influence on the tissue structure of the vessel wall and it is likely that high WSS affects the aneurysm initiation. The WSS represents the tangential force produced by blood moving across the vessel surface. However, the influence of WSS to the aneurysm progression or the risk of rupture is discussed controversially (see Moore et al. [25] for a numerical computation of WSS.). Similar to WSS, the *flow pressure* is considered as a relevant attribute for aneurysm initiation (it affects the vessel wall weakening) and progression (see Tritton [36] for a numerical computation of the pressure). An important influence on the risk of rupture has the *inflow jet* characterized by its width and impingement size. Ruptured aneurysms were more likely to have narrow inflow jets with small impingement regions [10].

Global Scope		Near-Wall Scope		Aneurysm Scope	
Focus	Context	Focus	Context	Focus	Context
Flow	Pressure	WSS/ Pressure	WSS/ Pressure/ Flow	Flow	Vorticity In- and Outflow Inflow Jet

Table 1. Overview of the three spatial scopes with corresponding pairs of hemodynamic attributes that are relevant for the visual exploration.

5.2 Spatial Scopes With Hemodynamic Attributes

The identified hemodynamic attributes refer to three spatial scopes which comprise the near-wall flow, embedded flow and anatomy-guided flow exploration from Sec. 3.3. We assign the attributes to each scope and compose them to pairs of hemodynamic focus-and-context attributes as follows (see also Table 1):

Global Scope: The global scope consists of the embedded flow as focus attribute. It describes the flow behavior in the parent vessel as well as in the aneurysm and is characterized by the flow direction and velocity. A more detailed view onto the flow pattern can be achieved by incorporating flow pressure as context attribute, e.g., to investigate the parabolic flow profile and pressure distributions near to the vessel wall.

Near-Wall Scope: Investigations of near-wall information are relevant for aneurysm initiation and progression. Thereby, WSS and surface pressure are considered as focus attributes. To depict the correlation of both attributes to each other, we define WSS and surface pressure as alternate context attributes. Domain experts are also interested in the underlying flow of vessel regions where values of high and low WSS as well as surface pressure occur. Hence, we define the local flow as additional context attribute.

Aneurysm Scope: The flow characteristic within the aneurysm is relevant in terms of the risk of rupture. Based on the inflow and outflow of the aneurysm as focus attribute, additional visual information about the degree of vorticity, the amount of inflow and outflow at the ostium as well as the shape of the inflow jet is of interest. A shape description of the inflow jet provides also hints about the size of the impingement region at the aneurysm wall.

5.3 The FLOWLENS

We aim at an interactive focus-and-context approach with a simple interaction scheme and a flexible filtering of hemodynamic attributes. We present the FLOWLENS as a 2D focus-and-context approach that fulfills these requirements. Within the lens, additional hemodynamic context attributes are shown based on a current focus attribute. We thus achieve a high density of information in the lens region, where foveal vision occurs. In the following, we present the details.

5.3.1 Dimensionality

Existing lens techniques can be categorized in 2D, 2.5D and 3D. In the following, we discuss advantages and disadvantages of each category in terms of flow field exploration.

2D: A 2D lens consists of a 2D shape which is placed in the image plane and based on the magic lens approach (recall Bier et al. [4]). The lens transformation (movement, scaling, rotation) is restricted to the 2D image plane and can be easily manipulated by a 2D input device (mostly a mouse). Each visual style for the objects within the lens shape can be rendered in individual buffers and composed in a fragment shader. The manipulation of the lens content enables visual filtering of the flow by suppressing distracting information. However, probing a 3D flow field is not possible due to the missing spatial correlation between the 2D position of the lens and the 3D dataset.

2.5D: A 2.5D lens consists of a 2D shape which is placed and aligned in 3D (e.g., a cross-section plane). Its position has a spatial correlation to the 3D flow dataset and can be used as seeding location for streamlines and pathlines as well as probing location for specific flow attributes. In contrast to a 2D lens, the movement and rotation of a 2.5D lens is extended to 3D. However, this leads to an increased interaction effort to place and align the lens within
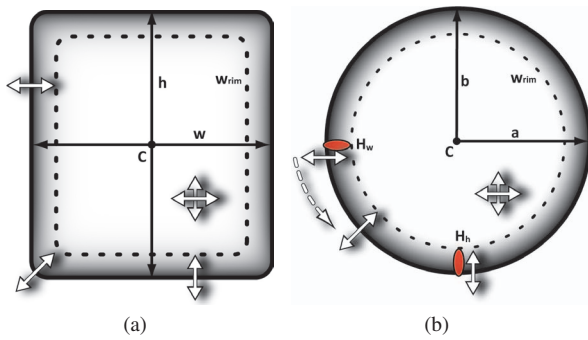
Fig. 3. Illustration of the lens shape: (a) rectangular and (b) ellipsoidal. The transformation options are indicated through arrows. For the ellipsoidal shape, the handles are enhanced in red.

the 3D dataset. One-click strategies [37] or guidance strategies [28] based on centerlines or anatomical axes may be incorporated to support the placement. Additionally, the application of visual filters to flow subvolumes or their investigation are not useful due to the 2D restriction of the lens shape.

3D: A 3D volumetric lens (recall Viega et al. [38]) is an extension of the 2.5D lens. In contrast to a 2.5D lens, a 3D lens consists of a 3D volume (e.g., a sphere or a box) on which visual or geometrical filters can be applied. The placement of a 3D lens suffers from the same interaction effort like a 2.5D lens. Guidance strategies, such as snapping or advanced manipulation schemes [32], must be provided to support the placement.

Since simplicity is a major requirement, we decided to employ a 2D lens for the visual filtering. This is also motivated by the observation that medical experts are familiar with 2D tools, like magnifying lenses or rulers, in their clinical workstations. Additionally, we incorporate a 2.5D lens within the 2D lens to enable probing and slicing through the aneurysm flow. The probing plane is view aligned and restricted to the 2D lens shape. It can be moved interactively through the flow volume to ensure the spatial correlation.

5.3.2　Lens Design

We provide two common lens shapes: a simple rectangular shape (see Fig. 3(a)) and an ellipsoidal shape (see Fig. 3(b)). The rectangular shape has a center $\mathbf{C}$, a width $\mathbf{w}$ and a height $\mathbf{h}$. The shape of the ellipsoidal lens is defined by a center $\mathbf{C}$ as well as by a major and minor radius $\mathbf{a}$ and $\mathbf{b}$. The borders of both shapes are depicted by a single color line or by a translucent transition zone defined by a rim width $\mathbf{w}_{rim}$. We define $\mathbf{w}_{rim}$ as $[0.95 \cdot d, d]$ with d as Euclidean distance from the center to the borders. Furthermore, the ellipsoidal shape consists of two handles (red) to indicate one of the possible interaction schemes described in the next subsection.

5.3.3　Lens Interaction

The lens provides several interaction possibilities which consist of the lens transformation, manipulating the focal point of the camera, probing facilities as well as observing hemodynamic changes over time.

Transformation: Lens transformation is performed in a straightforward manner. The width and height of the rectangular shape can be adjusted by simply clicking and dragging one of the corresponding edges. Uniform scaling is performed by dragging one of the corners (see Fig. 3(a)). The major and minor radii of the ellipsoidal shape can be modified by clicking and dragging handles $\mathbf{H}_a$ and $\mathbf{H}_b$. Furthermore, if the mouse translation also incorporates an up and down or left and right movement, a simultaneous rotation around $\mathbf{C}$ is possible. Uniform scaling is achieved by clicking and dragging of the contour line (see Fig. 3(b)). For both shapes, translation is performed by clicking and dragging the inside of the lens.

Center of Camera Rotation Displacement: If the lens is moved to a particular region of interest and a context attribute is shown, the user may rotate the camera around this region to investigate the current focus-and-context correlation from different views. In most cases, the center of the camera rotation, defined by the focal point, does not match with the center of the region of interest. Hence, we provide a displacement of the focal point to the current region of interest. The new focal point is located on the surface point of the context attribute underneath the lens center. This point is determined by the first hit point of the intersection between a ray and the attribute surface representation. The ray is defined by the world position of the lens center and the camera position.

Probing: Probing is provided by placing a view-aligned 2.5D plane within the lens. Parts of the plane which are outside the lens are masked. The plane can be sliced by the user through the volume grid where specific hemodynamic attributes can be resampled. The initial position of the plane corresponds to the intersection point of the ray and the vessel surface, as described for displacing the focal point. The plane normal is given by the normalized ray direction. The spatial extension of the probe plane is restricted to the lens shape as well as to the inside of the cut contour.

Observing Changes Over Time: Since we also deal with time-dependent flow data, a facility to explore hemodynamic changes over time is provided. Based on the current context visualization within the lens, the progression of the context attribute can be observed by slicing through the time steps. In each step, the context visualization is updated to the current value of the context attribute.

6　FLOWLENS VISUALIZATION TEMPLATES

We now present the visualization of the spatial scopes with their pairs of hemodynamic focus-and-context attributes (recall Sec. 5.2). Each scope consists of pairs of focus vs. context attributes and we propose visualization templates to represent each pair. The FLOWLENS is used to accomplish a visual distinction between focus-and-context attributes. By default, the current focus attribute is visualized outside and inside the lens. For the visual correlation to a context attribute the lens can be moved to the region of interest and the visualization of the context attribute is incorporated into the lens. Thereby, the focus attribute is attenuated to avoid occlusions and visual clutter. The transition zone is used to blend smoothly between the focus-and-context visualization. We first describe the visualization of the focus attributes and subsequently the combination to the context attributes.

6.1　Global Flow Scope

For visualizing the embedded flow as focus attribute, we employ color-coded streamlines for steady flow as well as pathlines for unsteady flow. For the line propagation process we need to place seed points. These seed points implicitly influence which part of the flow will be visible. Since the flow at the aneurysm is essential, we automatically place a seed sphere at point P_{seed} of the parent vessel centerline. This point denotes the middle of the centerline section below the ostium (see Fig. 4(a)). The endpoints of this section result from the ostium extraction method described in [26]. The radius of the seed sphere is defined by the maximum inscribed sphere radius at P_{seed}. Within
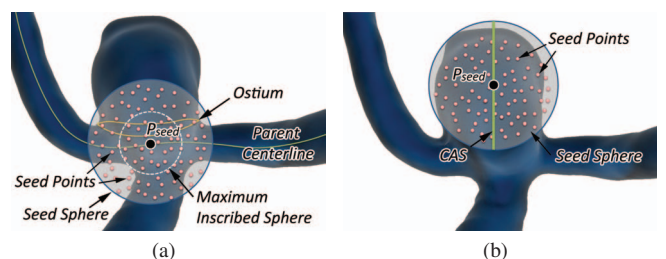

Fig. 4. Seed point strategies: (a) for the line propagation in the global flow scope, (b) for the inflow jet extraction in the aneurysm scope.
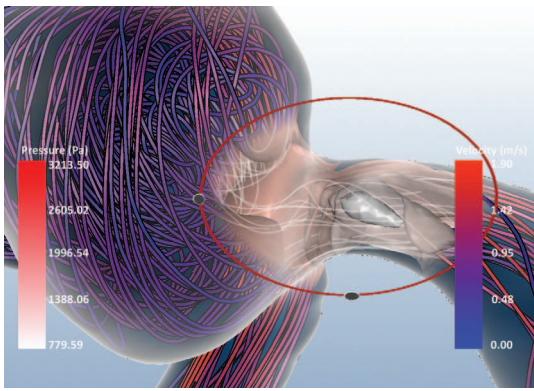
Fig. 5. Flow vs. pressure attribute: the flow (focus) is depicted with illustrative streamlines. Within the FLOWLENS the flow pressure (context) is depicted as isosurfaces and the flow as thin streamlines.

Fig. 7. Surface pressure vs. flow attribute: the surface pressure (focus) is shown as color-coded surface rendering. Within the FLOWLENS the flow (context) is embedded as illustrative streamlines and the pressure is indicated by saturation-coded contour lines (green).

the seed sphere we uniformly distribute seed points at which the line propagation starts in forward and backward direction. The number of seed points can be adjusted by the user. In terms of the color coding, we employ a blue-to-red color mapping of the velocity. This is a familiar color scale for low and high velocity values. Furthermore, we incorporate depth-dependent halos to increase the spatial perception of the generated lines (see Fig. 11(a) and (b)). Additionally, the user may provide a value to adjust the number of visible lines. Since spatial context of the enclosing vessel surface is important for the exploration, we employ the ghosted view approach of Gasteiger et al. [15] (see Fig. 5).

6.1.1 Flow vs. Pressure

To provide information about flow pressure as context, we employ an isosurface representation of the pressure values within the lens. Domain experts employ this kind of visualization method to extract structures of specific 3D scalar values, e.g., density values in medical image datasets. The isosurface extraction is based on a user-defined range of isovalues. If multiple isovalues are used we apply a white-to-red color map as an ordinal color map, to distinguish low and high pressure surfaces. Ordinal color maps are necessary to convey the ordinal data characteristics of scalar values. Within the lens, the visualization of the flow is attenuated by thin and semi-transparent line renderings to avoid visual clutter (see Fig. 5).

6.2 Near-Wall Scope

The focus attributes of near-wall information are WSS and surface pressure as 2D scalar values onto the vessel surface. Thereby, we consider only one surface attribute at once for the focus visualization. As

an established visualization method for 2D surface data we use color coding for both attributes. We apply a split color map to provide a distinction between normal and increased magnitude. Values below a user-defined threshold are mapped to a white and values above are mapped to a yellow-to-red color map. This color map represents the ordinal data characteristic of both attributes and red is an established signal color for critical values.

6.2.1 WSS vs. Surface Pressure

If one of the focus attributes is considered as context attribute, a color coding of both attributes leads to visual clutter. Instead, we overlay the color-coded focus attribute with a contour plot of the context attribute within the lens (see Fig. 6). The contour extraction is again based on a user-defined range of iso-values. If multiple contour lines have been extracted, we apply the same ordinal color map as for context visualization of the flow pressure. The spatial context inside and outside the lens is depicted as opaque surface rendering.

6.2.2 WSS and Surface Pressure vs. Flow

To provide context information within the lens about the underlying flow, we display the streamline or pathline visualization of the flow from Sec. 6.1. The enclosing vessel surface is depicted with the ghosted view rendering (recall [15]) to reveal the embedded line visualization as well as to enhance shape perception of the enclosing surface. Furthermore, we provide a contour plot of the current focus attribute (WSS or surface pressure) as attenuated focus information. The contour plot is adjusted by a user-defined threshold (see Fig. 7).

6.3 Aneurysm Scope

The focus attribute for the aneurysm flow scope is the inflow and outflow of the aneurysm. We depict the flow with the depth-enhanced streamline or pathline visualization. In contrast to the seeding strategy for the embedded flow, we use the mesh vertices of the extracted ostium as seeding location. Thus, the flow visualization is restricted to flow that runs in and out of the aneurysm through the ostium. This restriction is essential to evaluate the overall inflow and outflow condition. Furthermore, the ostium extraction method we used [28], ensures a regular distribution of the mesh vertices to avoid fixed structures of the traced streamlines and pathlines. To adjust the number of lines, we provide a user-defined ratio value to employ only a subset of the ostium vertices as seed point.
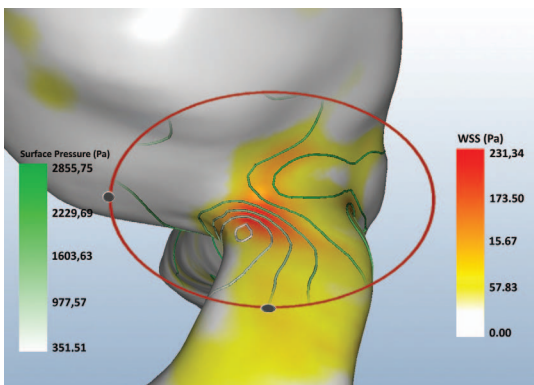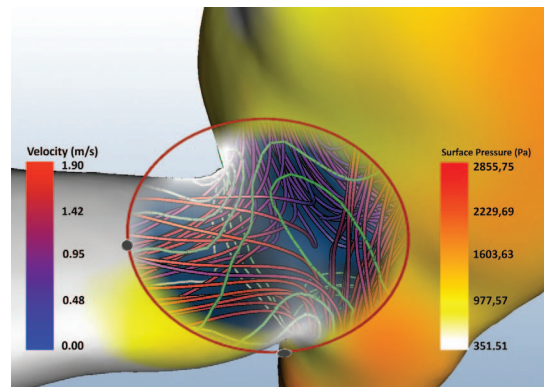

Fig. 6. WSS vs. surface pressure attribute: the WSS (focus) is depicted as color-coded surface rendering. Within the FLOWLENS the pressure (context) is enhanced as saturation-coded contour lines (green).

6.3.1 Flow vs. Vorticity

To depict the vorticity as context information, we employ the view-aligned probe plane of the lens combined with a color-coded LIC visualization of the resampled flow. The coloring encodes the velocity and is mapped to the blue-to-red color map as used for the streamlines and pathlines. Due to the dense representation of the LIC, a detailed
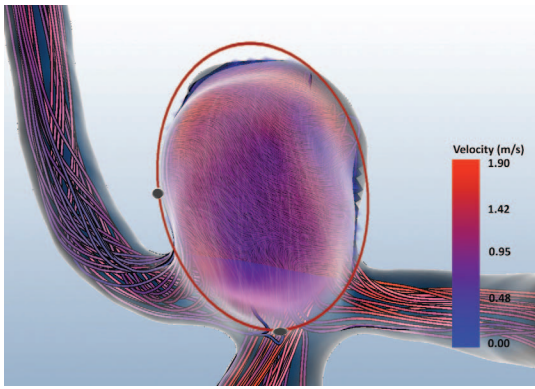
Fig. 8. Flow vs. vorticity attribute: the flow (focus) is depicted with il-lustrative streamlines. Within the FLOWLENS the vorticity (context) is depicted by a color-coded LIC and the streamlines are attentuated.

Fig. 10. Flow vs. inflow jet attribute: within the FLOWLENS the inflow jet (context) is depicted with color-coded glyphs and the flow (focus) is attenuated with thin and semi-transparent streamlines.

view onto the degree of the local vorticity is achieved. Furthermore, if the probe plane orientation is nearly coplanar to the CAS axis of the aneurysm, the color coding conveys the inflow jet size, since the inflow velocity is always higher than the outflow velocity. However, the 3D extension of the jet cannot be depicted due to the reduction to 2D. Hence, we provide a more expressive depiction of the inflow jet in Sec. 6.3.3. To convey the inflow, we extend the context visualization by a thin and semi-transparent line rendering of the flow (see Fig. 8). The vessel context is conveyed by the ghosted view rendering.

6.3.2 Flow vs. In- and Outflow

The context information of the in- and outflow condition at the ostium consists of the local velocity as well as the inflow and outflow region. The velocity is color-coded on the ostium using the blue-to-red ve-locity encoding. To separate the inflow from the outflow region, we first compute the normalized volumetric flow rate $\hat{R}_i$ for each of the k triangle elements of the ostium:

$$\hat{R}_i = \left(A_i (\vec{v}_i \cdot \vec{n}_i) \sum_{i=0}^{k} R_i \right) / |R_{\max}|. \tag{1}$$

Where A_i is the element area, v_i and n_i are the flow vector and normal of the element as well as R_{max} as the maximum element-wise volu-metric flow rate. The normalization is necessary, since the volumetric flow rate is area-dependent. It ensures that the computed flow rate is independent of the ostium mesh tessellation. Because $\hat{R}_i$ is signed, the inflow (positive) and outflow (negative) region can be separated by finding the zero-crossing. We use a red-colored contour line to depict
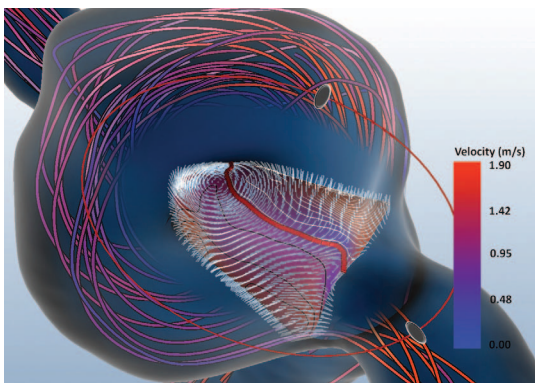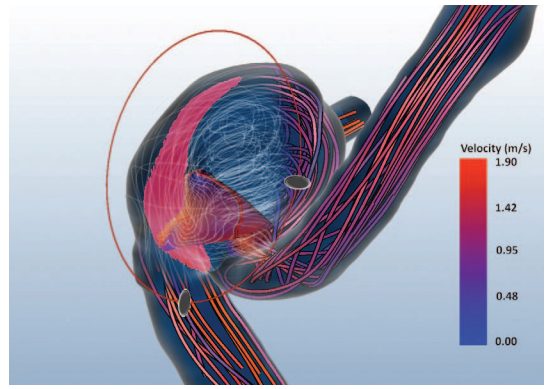

Fig. 9. Flow vs. in- and outflow attribute: within the FLOWLENS the in- and outflow at the ostium (context) is separated by a red contour line. The flow at the ostium is indicated by short streamlines.

the separation line, as shown in Fig. 9. To enhance the separation, we overlay the inflow and outflow region with color-coded contour lines. We use a binary color scheme with white for inflow and black for out-flow lines to reduce a visual interference with the color-coded velocity on the ostium mesh. Furthermore, we provide a depiction of the flow direction at the ostium based on short streamlines or pathlines seeded from the vertices of the ostium mesh. This reveals details about the flow behavior near the ostium. To minimize occlusions to the under-lying context visualization, the lines are semi-transparently rendered without color coding. An example is given in Figure 9, where near to the inflow-to-outflow separation line a vortex structure is shown.

6.3.3 Flow vs. Inflow Jet

The inflow jet as context information to the inflow is defined as inflow with high velocity. The visualization of the jet has to convey the 3D extension of the jet size. We first provide the ostium mesh as anatomic landmark, which is color-coded in terms of the velocity and is overlaid with the inflow and outflow separation line as described in Sec. 6.3.2. To depict the inflow jet, we employ a 3D glyph-based visualization, based on a dense line seeding strategy within the aneurysm. We place a seed sphere at point P_{seed}, centered on half of the central aneurysm axis (CAS) (recall Sec. 3) with radius $|CAS|/2.0$ (see Fig. 4(b)). The radius ensures that the seeding sphere contains the whole aneurysm. Within the sphere, we randomly distribute a dense amount of points used as seeding points for a streamline or pathline propagation pro-cess. We filter lines with a velocity less than a user-defined velocity threshold. At each remaining line vertex we place a hedgehog glyph oriented according to the local line direction. Finally, the glyphs are color-coded according to the velocity encoding of the ostium mesh. To convey the surrounding flow pattern, we provide a thin and semi-transparent line rendering of the inflow, as described in Sec 6.3.1. The final focus-and-context visualization is shown in Figure 10.

6.4 Implementation

The implementation of the FLOWLENS visualization templates is straightforward and based on the Visualization Toolkit (VTK) as well as the prototyping environment MEVISLAB. We render the focus vi-sualization and the additional context visualization in two offscreen buffers using the standard visualization techniques. The lens is ren-dered in two additional buffers. In one buffer, the lens shape is stored as blending mask with white as inside the lens and black as outside. The transition zone is encoded as black-to-white gradient. The second lens buffer consists of the color information of the lens appearance (contour line and handles). In a subsequent fragment shader, we lin-early blend between the two visualizations of the focus-and-context attribute by employing the blending mask. Thereby, full white cor-responds to an opaque rendering of the context visualization and full black to the focus visualization. Within the transition zone both vi-sualizations are smoothly blend. The lens appearance is rendered as
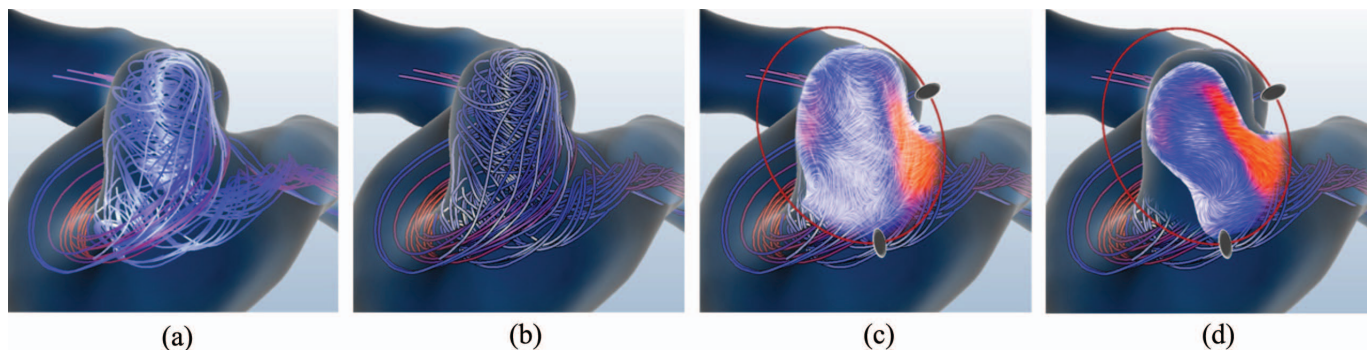
Fig. 11. Overview of the FLOWLENS application in the aneurysm scope. In (a) the inflow and outflow is depicted with illuminated streamlines. The spatial perception of the flow pattern is enhanced by (b) incorporating depth-dependent halos. For a detailed view of the internal vorticity, the FLOWLENS shows (c) a LIC visualization on a view-aligned probe plane (d) which can be sliced through the flow volume.

overlay onto the resulting visualization.

7 RESULTS AND INFORMAL USER FEEDBACK

We employed seven flow datasets to evaluate our approach. For five datasets, the flow was derived from CFD simulations based on clinical patient scans. For two datasets, we employed an aneurysm phantom dataset with three artificial aneurysms where the flow was obtained by a CFD simulation and from a measurement with a 7 Tesla 4D PC-MRI scan (spatial resolution: $144 \times 256 \times 128$, voxel size: $1 \times 1 \times 1$mm, temporal resolution: 107ms). The measured flow data was linearly interpolated onto the CFD volume grid. The first five datasets are steady flow and the two phantom datasets represent unsteady flow with 10 time steps. On our prototypic system, the preprocessing time of the datasets ranges from 10 to 40 sec on a mid-class desktop computer (Core 2 Duo 3.16GHz, 8GB RAM, nVidia GeForce 9800 GT). The preprocessing includes dataset loading, the extraction of the ostium as well as streamline and pathline tracing. The density filtering of the resulting lines, the viewpoint changes, the adjustment of color schemes as well as the FLOWLENS interaction and blending, could be performed at interactive rates. However, the update rate of the LIC generation and time slicing are not interactive.

7.1 Results

In Figure 11, an overview of the FLOWLENS application in the aneurysm scope is presented. The flow as focus attribute is depicted with illuminated streamlines in Fig. 11(a), where the velocity is color-coded according to Sec. 6.1. Since the vertices of the ostium mesh are used to seed the streamlines, only the inflow and outflow of the aneurysm is depicted. In the current example, the ostium mesh consists of 395 vertices from which we only employ every fifth as seed point to reduce the amount of lines. For comparison, the streamlines in Fig. 11(b) are enhanced by using halos. In both images, the turbulent flow pattern within the aneurysm is visible. However, the spatial perception of individual lines is increased by the halos, as can be seen for the helical outflow in the parent vessel. To present a detailed view on the flow pattern at a region of interest, the FLOWLENS (green) is placed in Fig. 11(c) and the vorticity is depicted by a LIC plane within the lens. The plane is placed according to the probing facility of the FLOWLENS and overlaid by a color coding of the velocity. The plane is set back in Fig. 11(d) to illustrate the 3D slicing capability.

As a demonstration of the time slicing possibility of the FLOWLENS, a sequence of pathlines is shown in Figure 12. In the left image, the flow for one time step of the cardiac cycle is shown by depth-dependent streamlines. The visualization depicts a helical flow structure within the aneurysm. To investigate the development of this flow feature, the FLOWLENS is placed over the aneurysm. Within the lens shape, a sequence of pathlines over three time steps is shown, capturing a time frame of 214ms up to 1075ms within the cardiac cycle. The restriction of the time-varying visualization to the lens shape minimizes visual clutter and draws attention to the region of interest.

7.2 Informal User Feedback

To gain a qualitative user feedback, we conducted three informal interviews with two clinicians and one biomedical researcher who are actively involved in the exploration of cerebral or cardio-vascular blood flow. They were not involved in the FLOWLENS design. The interviews were designed to determine if the requirements in Sec. 4 were principally met and which details might need an improvement. Each interview was divided into two parts. The first part consisted of an introduction of the FLOWLENS. Each expert had to evaluate the lens design and its transformation options (translation, scaling, rotation). All experts considered the interaction as intuitive since it is similar to daily used 2D tools like 2D measurement tools. Especially the rotation capability of the ellipsoidal lens shape was valued as useful to adapt the lens region to relevant anatomic structures. However, one clinician stated an increased effort to adjust a specific ellipsoidal shape and prefers a circular shape with uniform scaling.

In the second part of the interview, we presented the three spatial scopes subsequently. For each scope, the focus attribute was shown at first and then individual context attributes could be investigated within the lens. During the presentation of a particular scope, the experts had to evaluate the amount of visual information, the visualization of the individual attributes and the interaction as well as the usefulness of the FLOWLENS.

For the global scope, all experts stated an improved spatial perception of the streamlines and pathlines with depth-dependent halos in comparison to a standard illuminated line rendering. The improved perception was most clearly if the camera has zoomed closer to the lines. One expert preferred the pure illuminated line rendering for the investigation of the velocity distribution. He noticed that the halos occluded some parts of underlying lines which caused a decreased perception of the velocity color-coding. All experts rated the adjustment of the number of lines as very useful and the blue-to-red color map as intuitive. All experts stated the need for a color legend to map color values to numerical values. After an overall investigation of the flow attribute, one clinian employed the FLOWLENS for a specific and typical task. He placed the lens over a surface region at the ostium to investigate the local pressure distribution. Thereby, the corresponding isosurface rendering was initially not comprehensible but became clear after a short explanation. During the exploration, one expert preferred a low number of extracted isosurfaces and the exclusion of the thin and semi-transparent flow lines as the attenuated focus attribute. The visual information was too complex and not necessary for him. Additionally, he preferred a more saturated color distinction of different pressure levels. The biomedical researcher valued the pressure isosurfaces as useful to convey the parabolic flow profile, especially the restriction of the pressure visualization to the lens content. He agreed that an integrated visualization of flow lines and pressure is disturbing and he suggested to display them on demand. All experts preferred a more saturated color distinction
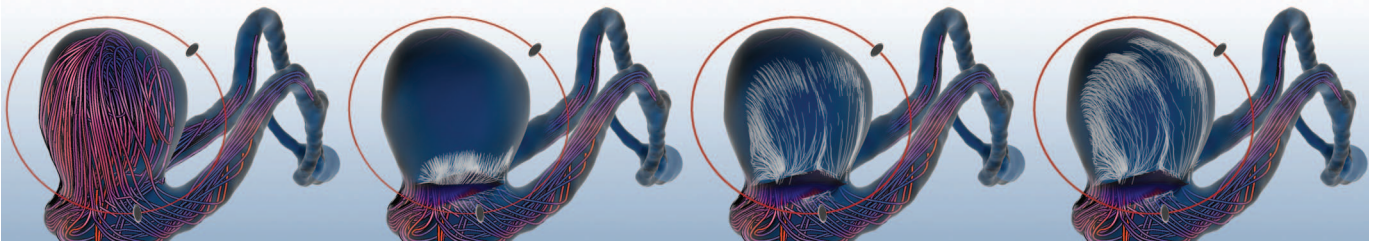
Fig. 12. Example of the time slicing possibility of the FLOWLENS. The lens is placed over the aneurysm (left) and a sequence of pathlines over three time steps is depicted within the lens. The time steps capture a time frame of 1075ms. Outside the lens, the flow is visualized with streamlines.

of the different pressure levels. The focal point displacement by the FLOWLENS was valued as very useful by all three experts. It simplifies the investigation of the focus and context attribute from different view points by reducing the number of camera adjustments. In terms of the near-wall scope, all three experts denoted the WSS and surface pressure as important focus attributes. The correlation of WSS or surface pressure to the underlying flow as context attribute was comprehensible. For example, one expert placed the FLOWLENS over a region of high WSS to validate a high velocity distribution of the underlying flow. However, the contour lines of WSS or surface pressure within the lens was valued as disturbing since the flow was also depicted with lines.

The most interesting spatial scope for both experts was the aneurysm scope. Two experts rated the depiction of the vorticity by the view-aligned LIC plane within the FLOWLENS as intuitive and comprehensible, especially the depth slicing of the plane. However, all three experts denoted the visual information within the lens as too complex due to the additional depiction of the ostium and the flow. These information should be optional (see Fig. 11)(d). The overall separation of the inflow and outflow region at the ostium was rated as important to visually assess the amount and location of inflow and outflow. In terms of enhancing the separation by the contour lines, two experts suggested a more discrete distinction, e.g., a discrete color map or an inflow and outflow arrow glyph. Again, the experts suggested to provide the short and semi-transparent streamlines at the ostium optionally and a color legend about the contour lines is necessary. According to the inflow jet, all three experts rated the glyph representation as intuitive and depicted the 3D shape well. For this context attribute, the displacement of the focal point by the FLOWLENS as well as the rotation of the ellipsoidal shape were rated as useful to investigate the jet shape from different views. For the two clinicians it was quite interesting to get an impression of the impingement zone at the aneurysm wall.

All three experts valued the time slicing capability in each scope and its restriction to the lens content as useful. It draws the attention to a certain focus region where changes of the context attribute can be observed. In terms of the transition zone, the two clinicians preferred a clear border of the FLOWLENS. They argued that a smooth transition zone attenuate the values at this region and can lead to a misinterpretation.

8 CONCLUSION

We presented a focus-and-context visualization approach to explore hemodynamic data in cerebral aneurysms. The qualitative analysis of these data involves the investigation of focus-and-context attributes at different spatial scopes. We identified relevant pairs of hemodynamic focus-and-context attributes and assigned them to different anatomic scopes: global, near-wall and aneurysm. For each scope we proposed several visualization templates to depict the corresponding focus attributes and additional context attributes. The FLOWLENS was introduced to enable a flexible visual filtering between these attributes. The placement of the lens occurs in 2D and provides several interaction possibilities, like a 2.5D probing with the volumetric flow data. For the visualization templates, we employed depth-dependent streamlines and pathlines as well as LICs, which are applicable to steady and un-

steady flow data. Although our work was focused on the exploration of cerebral aneurysms, we believe that it can be transferred to support the treatment of other vascular diseases, in particular diseases where the coronary arteries are involved and an understanding of the flow is also important (see also Markl et al. [23]).

The qualitative evaluation within the frame of informal user interviews confirmed the general usefulness of the aggregation of hemodynamic focus-and-context pairs and their assignment to the presented spatial scopes. The experts valued the FLOWLENS as an intuitive exploration tool to support a flexible visual filtering and the investigations of hemodynamic correlations. This user feedback provides a valuable basis for further research in terms of a *quantitative evaluation*. The design of this user study will be oriented at the work of Laidlaw et al. [20]. The FLOWLENS approach will be compared with a standard side-by-side view and a multiparameter visualization without focus-and-context mechanism. For this comparison the participants have to fulfil representative tasks that domain experts want to perform from visualizations. This will include finding of regions with elevated near-wall velocity and WSS, identifying and describing the inflow jet and its impingement zone as well as counting the number of critical points and evaluating their stability within the aneurysm. The three different visualization approaches will be evaluated with respect to the participants' accuracy, response time, and their personal preferences.

Furthermore, it would be worthwhile to investigate how effective and expressive seeding strategies can be incorporated during the visual exploration. In its current state, our approach used a fixed seed point strategy (e.g., the ostium). However, it might be of interest to provide a flexible seeding in the parent vessel or the aneurysm to trace the flow in detail within the FLOWLENS. To cope with the high visual complexity of streamlines and pathlines, flow clustering techniques could be used to create expressive and more abstract flow representations. The FLOWLENS can then be used to reveal the flow in the lens region.

REFERENCES

[1] N. Andaluz and M. Zuccarello. Recent Trends in the Treatment of Cerebral Aneurysms: Analysis of a Nationwide Inpatient Database. *Neurosurgery: Pediatrics*, 108(6):1163–1169, 2008.

[2] S. Appanaboyina, F. Mut, R. Löhner, C. Putman, and J. Cebral. Computational Fluid Dynamics of Stented Intracranial Aneurysms Using Adaptive Embedded Unstructured Grids. *Numerical Methods in Fluids*, 57(5):475–493, 2008.

[3] L. Augsburger, P. Reymond, E. Fonck, Z. Kulcsar, M. Farhat, M. Ohta, N. Stergiopulos, and D. Rüfenacht. Methodologies to Assess Blood Flow in Cerebral Aneurysms: Current State of Research and Perspectives. *Neuroradiology*, 36(5):270–277, 2009.

[4] E. A. Bier, M. C. Stone, K. Pier, W. Buxton, and T. D. DeRose. Toolglass and Magic Lenses: The See-Through Interface. In *Proceedings of SIGGRAPH*, pages 73–80, 1993.

[5] S. Born, A. Wiebel, J. Friedrich, G. Scheuermann, and D. Bartz. Illustrative Stream Surfaces. *IEEE Transactions on Visualization and Computer Graphics*, 16(6):1329–1338, 2010.

[6] L. Boussel, V. Rayz, A. Martin, G. Acevedo-Bolton, M. T. Lawton, R. Higashida, W. S. Smith, W. L. Young, and D. Saloner. Phase-Contrast Magnetic Resonance Imaging Measurements in Intracranial Aneurysms In Vivo of Flow Patterns, Velocity Fields, and Wall Shear Stress: Comparison with Computational Fluid Dynamics. *Magnetic Resonance Imaging in Medicine*, 61:409–417, 2009.

[7] R. D. Brown, J. Huston, R. Hornung, T. Foroud, D. F. Kallmes, D. Kleindorfer, I. Meissner, D. Woo, L. Sauerbeck, and J. Broderick. Screening for Brain Aneurysm in the Familial Intracranial Aneurysm Study: Frequency and Predictors of Lesion Detection. *Neurosurgery: Pediatrics*, 108(6):1132–1138, 2008.

[8] R. Bürger and H. Hauser. Visualization of Multi-Variate Scientific Data. In *Proceedings of EuroVis*, pages 117–134, 2007.

[9] J. R. Cebral, M. A. Castro, J. E. Burgess, R. S. Pergolizzi, M. J. Sheridan, and C. M. Putman. Characterization of Cerebral Aneurysms for Assessing Risk of Rupture by Using Patient-Specific Computational Hemodynamics Models. *American Journal of Neuroradiology*, 26(10):2550–2559, 2005.

[10] J. R. Cebral, F. Mut, J. Weir, and C. M. Putman. Association of Hemodynamic Characteristics and Cerebral Aneurysm Rupture. *American Journal of Neuroradiology*, 32(2):264–270, 2011.

[11] J. R. Cebral, F. Mut, J. Weir, and C. M. Putman. Quantitative Characterization of the Hemodynamic Environment in Ruptured and Unruptured Brain Aneurysms. *American Journal of Neuroradiology*, 32(1):145–151, 2011.

[12] I. Chatziprodromou, V. D. Butty, V. B. Makhijani, D. Poulikakos, and Y. Ventikos. Pulsatile Blood Flow in Anatomically Accurate Vessels with Multiple Aneurysms: A Medical Intervention Planning Application of Computational Hemodynamics. *Flow, Turbulence and Combustion*, 71(1):333–346, 2003.

[13] A. Cockburn, A. Karlson, and B. B. Bederson. A Review of Overview+Detail, Zooming, and Focus+Context Interfaces. *Computing Surveys*, 41:2:1–2:31, 2009.

[14] M. H. Everts, H. Bekker, J. B. Roerdink, and T. Isenberg. Depth-Dependent Halos: Illustrative Rendering of Dense Line Data. *IEEE Transactions on Visualization and Computer Graphics*, 15(6):1299–1306, 2009.

[15] R. Gasteiger, M. Neugebauer, C. Kubisch, and B. Preim. Adapted Surface Visualization of Cerebral Aneurysms with Embedded Blood Flow Information. In *Proceedings of VCBM*, pages 25–32, 2010.

[16] A. Hennemuth, O. Friman, C. Schumann, J. Bock, J. Drexl, M. Markl, and H.-O. Peitgen. Fast Interactive Exploration of 4D MRI Flow Data. In *Proceedings of SPIE Medical Imaging*, 2011.

[17] Y. Hoi, S. H. Woodward, M. Kim, D. B. Taulbee, and H. Meng. Validation of CFD Simulations of Cerebral Aneurysms with Implication of Geometric Variations. *Biomechanical Engineering*, 128:844–851, 2006.

[18] S. Juvela, M. Porras, and K. Poussa. Natural History of Unruptured Intracranial Aneurysms: Probability of and Risk Factors for Aneurysm Rupture. *Neurosurgery*, 93(3):379–387, 2000.

[19] J. Krüger, J. Schneider, and R. Westermann. Clearview: An Interactive Context Preserving Hotspot Visualization Technique. *IEEE Transactions on Visualization and Computer Graphics*, 12(5):941–948, 2006.

[20] D. H. Laidlaw, R. M. Kirby, C. D. Jackson, J. S. Davidson, T. S. Miller, M. da Silva, W. H. Warren, and M. J. Tarr. Comparing 2D Vector Field Visualization Methods: A User Study. *IEEE Transactions on Visualization and Computer Graphics*, 11(1):59–70, 2005.

[21] R. S. Laramee, H. Hauser, H. Doleisch, B. Vrolijk, F. H. Post, and D. Weiskopf. The State of the Art in Flow Visualization: Dense and Texture-Based Techniques. *Computer Graphics Forum*, 23(2):203–222, 2004.

[22] D. Lesage, E. D. Angelini, I. Bloch, and G. Funka-Lea. A Review of 3D Vessel Lumen Segmentation Techniques: Models, Features and Extraction Schemes. *Medical Image Analysis*, 13(6):819–845, December

2009.

[23] M. Markl, A. Harloff, T. A. Bley, M. Zaitsev, B. Jung, E. Weigang, M. Langer, J. Hennig, and A. Frydrychowicz. Time-Resolved 3D MR Velocity Mapping at 3T: Improved Navigator-Gated Assessment of Vascular Anatomy and Blood Flow. *Magnetic Resonance Imaging*, 25(4):824–831, 2007.

[24] O. Mattausch, T. Theußl, H. Hauser, and E. Gröller. Strategies for Interactive Exploration of 3D Flow Using Evenly-Spaced Illuminated Streamlines. In *Proceedings of SCCG*, pages 230–241, 2003.

[25] J. E. Moore, C. Xu, S. Glagov, C. K. Zarins, and D. N. Ku. Fluid Wall Shear Stress Measurements in a Model of the Human Abdominal Aorta: Oscillatory Behavior and Relationship to Atherosclerosis. *Atherosclerosis*, 110(2):225–240, 1994.

[26] M. Neugebauer, V. Diehl, M. Skalej, and B. Preim. Geometric Reconstruction of the Ostium of Cerebral Aneurysms. In *Proceedings of VMV*, pages 307–314, 2010.

[27] M. Neugebauer, R. Gasteiger, O. Beuing, and et al. Map Displays for the Analysis of Scalar Data on Cerebral Aneurysm Surfaces. *Computer Graphics Forum (EuroVis)*, 28 (3):895–902, 2009.

[28] M. Neugebauer, G. Janiga, O. Beuing, M. Skalej, and B. Preim. Anatomy-Guided Exploration of Blood Flow in Cerebral Aneurysms. In *Proceedings of EuroVis*, pages 1041–1050, 2011.

[29] P. Neumann, T. Isenberg, and S. Carpendale. NPR Lenses: Interactive Tools for Non-Photorealistic Line Drawings. In *Proceedings of Smart Graphics*, pages 10–22. Springer, 2007.

[30] A. M. Nixon, M. Gunel, and B. E. Sumpio. The Critical Role of Hemodynamics in the Development of Cerebral Vascular Disease. *Neurosurgery*, 112(6):1240–1253, 2010.

[31] T. Salzbrunn, H. Jänicke, T. Wischgoll, and G. Scheuermann. The State of the Art in Flow Visualization: Partition-Based Techniques. In *Proceedings of SimVis*, pages 75–92, 2008.

[32] R. Schmidt, K. Singh, and R. Balakrishnan. Sketching and Composing Widgets for 3D Manipulation. *Computer Graphics Forum*, 27(2):301–310, 2008.

[33] J. Schöberl. NETGEN An Advancing Front 2D/3D-Mesh Generator Based on Abstract Rules. *Computing and Visualization in Science*, 1:41–52, 1997.

[34] D. M. Sforza, C. M. Putman, and J. R. Cebral. Hemodynamics of Cerebral Aneurysms. *Annual Review of Fluid Mechanics*, 41:91–107, 2009.

[35] S. Tateshima, A. Chien, J. Sayre, J. R. Cebral, and F. Viuela. The Effect of Aneurysm Geometry on the Intra-Aneurysmal Flow Condition. *Neuroradiology*, 52(12):1135–1141, 2010. Published online.

[36] D. J. Tritton. *Physical Fluid Dynamics*. Clarendon Press, 1988.

[37] R. van Pelt, J. O. Bescós, M. Breeuwer, R. E. Clough, and E. Gröller. Exploration of 4D MRI Blood-Flow Using Stylistic Visualization. *IEEE Transactions on Visualization and Computer Graphics*, 16(6):1339–1347, 2010.

[38] J. Viega, M. J. Conway, G. Williams, and R. Pausch. 3D Magic Lenses. In *Proceedings of UIST*, pages 51–58, 1996.

[39] I. Viola and E. Gröller. Smart Visibility in Visualization. In *Proceedings of Computational Aesthetics*, pages 209–216, 2005.

[40] I. Viola, A. Kanitsar, and M. E. Gröller. Importance-Driven Feature Enhancement in Volume Visualization. *IEEE Transactions on Visualization and Computer Graphics*, 11(4):408–.418, 2005.

[41] L. Wang, Y. Zhao, K. Mueller, and A. E. Kaufman. The Magic Volume Lens: An Interactive Focus+Context Technique for Volume Rendering. In *Proceedings of IEEE Visualization*, pages 367–374, 2005.